Precipitation from Supersaturated Aluminate Solutions

I. Nucleation and Growth of Solid Phases at Room Temperature

H. A. VAN STRATEN, B. T. W. HOLTKAMP, AND P. L. DE BRUYN

Van 't Hoff Laboratorium, Transitorium 3, Padualaan 8, 3584 CH Utrecht, The Netherlands

Received May 19, 1983; accepted September 8, 1983

The precipitation of aluminum hydroxide from dilute potassium aluminate solutions ($10^{-4}\ M < C_{Al} < 16 \times 10^{-4}\ M$) was studied in acid titration and pH-stat experiments. In the relatively fast titrations a pseudo-equilibrium is obtained by formation of an amorphous phase. The precipitation behavior in pH-stat relaxation experiments is largely dictated by the supersaturation (II). At high supersaturations the precipitation sequence is amorphous-pseudoboehmite-bayerite and at low II only bayerite forms. Measurements of relaxation times reveal the precipitation boundary ($\log a_{H^+} \cdot a_{Al(OH)_4^-}$) for the amorphous phase (-12.1 ± 0.05) and for pseudoboehmite (-12.7 ± 0.1). The remarkable extrema in the relaxation time vs supersaturation curves are shown to indicate the retardation of the nucleation and growth of bayerite by heterogeneous nucleation of pseudoboehmite on the bayerite surface. A simple theoretical analysis of the dual role of pH, in determining both the supersaturation and the interfacial tension, shows that drastic changes in nucleation behavior can occur at pH values about 4 units away from the point-of-zero charge. The growth rate of bayerite in seeded and unseeded pH stat experiments is found to be second order in the aluminate concentration and somewhat less than second order in the hydrogen ion concentration. A brief discussion is given of a number of growth models which are consistent with the experimental growth rate expression.

INTRODUCTION

This is the first of a series of papers concerned with a systematic study of the nucleation and growth of aluminum hydroxides from supersaturated aluminate solutions.

The objectives of this study are twofold. Our first aim is to gain insight in the formation of the hydroxides in different chemical environments. In our research group the hydrolysis and subsequent precipitation of aluminum- and iron(III) hydroxides from acidic solutions have been extensively studied (1–3). Since aluminum hydroxide is amphoteric it can also be precipitated from basic solutions. We are therefore interested in comparing its precipitation behavior in a basic environment with that observed under acidic regimes.

Precipitation studies in a basic milieu has the distinct advantage that the hydrolysis reaction is less complicated compared to acid systems. In not too concentrated aluminate solutions the aluminate ion $Al(OH)_4^-$ is agreed to be the dominant solution species (4–6). Furthermore the precipitation products are also in general more crystalline (2) under these conditions. In the industrial Bayer process the production of large quantities of $Al(OH)_3$ is actually achieved in basic solutions. A fundamental study of precipitation in aluminate systems may therefore also prove to be of technological importance.

The second objective of this study is more model oriented. It is directed at an evaluation of the role of interfacial properties in nucleation and growth processes and in determining the physical character (crystallinity, habit, size, and uniformity) of the solid phase. The rate of nucleation is largely determined by two parameters, the degree of supersaturation (II) and the interfacial tension (σ). Adsorption of lattice or foreign ions may (drastically) change

0021-9797/84 $3.00

the magnitude of the interfacial tension and thereby alter the rate of nucleation. Direct measurements of the solid/liquid interfacial tension are not possible but often estimates of this property are obtained from nucleation studies (7). Adsorption of surface-active species is also known to influence the rate and the mechanism of crystal growth. The crystallization process may be retarded (8), the crystal habit of the precipitate may be changed significantly (9), and the polydispersity of the product may be controlled (10, 11) by addition of surface active species to the supersaturated solution.

By a proper choice of the physical and chemical environment during nucleation the different modifications of the solid phase may be induced to precipitate. If the system is supersaturated with respect to a number of different crystalline modifications, the thermodynamically least stable form is quite often the first one to form (12). This phenomenon known as the "Ostwald Rule of Stages" (13) can also be explained by kinetic arguments derived from nucleation theory (14). It is of importance in our study because at least four solid modifications of aluminum hydroxides are known to form at room temperature.

It is well-known that H^+ and OH^- act as potential-determining ions at the interface, solid hydroxide/aqueous solution (15). Excess adsorption of one of these ionic species determines the density and sign of the electrical charge carried by the solid surface and causes a lowering of the interfacial tension. In this publication emphasis will be laid upon the precipitation kinetics in supersaturated aluminate solutions at constant pH where we may assume the interfacial properties (charge, interfacial tension) to remain essentially constant during the nucleation and growth process. We report here on the influence of supersaturation degree, pH, ionic strength, and seeding on the precipitation behavior and on the nature of the precipitating solid phase. The products are to be characterized by X ray, infrared, BET, and electron microscopic techniques.

EXPERIMENTAL

Preparation of stock solutions. The potassium aluminate solutions used in the experiments were prepared by mixing solutions of $Al(NO_3)_3$ and KOH. Since poor mixing leads to formation of a solid phase which dissolves only slowly afterward all experiments were done with freshly diluted stock solutions prepared in the following reproducible way (2). A solution of 0.6 *M* $Al(NO_3)_3$ was injected under nitrogen pressure below the surface of a 1 *M* (CO_2-free) KOH solution with a Gilson peristaltic pump. This basic solution was stirred vigorously during the mixing process to ensure that the aluminum ions were directly exposed to a large excess of base and to avoid formation of a solid phase. The reaction vessel of special design has been described before (16). Addition of $Al(NO_3)_3$ was stopped at a final Al(III) concentration of 0.12 *M* and a $KOH/Al(NO_3)_3$ ratio of 6.5.

After 1 week storage in polyethylene bottles the stock solutions were pressure-filtered through millipore filters (pore size 0.65 μm) to remove solid impurities. Stock solutions prepared in this manner were stable (visually clear) for at least 2 years at room temperature. Storage and handling of the solutions were carried out so as to minimize dissolution of CO_2.

Acid titrations and pH-stat relaxations. Starting solutions were prepared by diluting a suitable amount of stock solution and adding a calculated amount of KNO_3 to reach the desired ionic strength. The final volume was always 3 liters. Both types of experiments were performed in the thermostatted reaction vessel referred to before. As titrant was used a HNO_3 solution of which the concentration was always chosen to equal 62.5 times that of the original aluminate. In this way the initial concentration of aluminate was decreased maximally by 6% and the dilution factor was the same in different experiments.

In the titration experiments the titrant solution was added at a constant speed. The pH

of the solution was registered as a function of time with an Ingold type HA 465-35-90 electrode in combination with an Orion pH meter and recorder. The constant pH relaxations were done with the aid of a Mettler pH-stat and an automatic burette which was connected to a recorder for registering the uptake of acid as a function of time. The same electrodes were used in these experiments. They contain an internal salt bridge which was necessary in order to obtain reproducible measurements. Calibration of the electrode was done before and after each experiment with Electrofact buffer solutions (pH values 6.98 and 9.18 at 25°C). The time required for building up the desired supersaturation in the pH-stat experiments was always less than 7 min.

In both types of experiments freshly twice-distilled water was used, the temperature was regulated at 25 ± 0.1°C, a nitrogen atmosphere was introduced to prevent uptake of CO_2, and analytical grade chemicals were used. A number of constant pH relaxations were performed in which a fixed amount of gibbsite seeds (10 g) was added just before the desired supersaturation was reached.

Characterization of the solid phase. Aliquots of the reacted solution were taken, then pressure-filtered through 0.65-μm Millipore paper. The solids were washed several times with twice-distilled water and air dried at room temperature and then characterized.

X-Ray diffraction measurements were carried out with a Debye–Scherrer camera by utilizing Cu$K\alpha$ radiation. In some cases the films were analyzed with a densitometer. Infrared analysis was done with a Hitachi EPI-G3 spectrophotometer employing KBr pellets. Surface area determinations were done with a Quantasorb apparatus (Quantachrome Corporation). The specific surface of each sample was obtained from measurements using three different N_2/He mixtures. Before making the surface area analysis the samples were washed until no nitrate could be detected in the infrared spectra and were outgassed for 0.5 to 1 hr at 80°C.

RESULTS

Titration Curves

A typical titration curve, pH versus OH/Al ratio, is given in Fig. 1. The OH/Al ratio is calculated from the identity, OH/Al = $[M_{KOH} - M_{HNO_3}]/M_{Al}$ where M_i is the amount of i in the system. At the start of an experiment this ratio is 6.5 and at the end it is 3 corresponding to complete neutralization of free alkali and precipitation of aluminate.

Figure 1 shows clearly that the titration curve may be divided into two regions. In region A the free base present in the system is neutralized and in region B the main reaction is the precipitation of $Al(OH)_3$. Visible precipitate is seen from the start in this region. We also note that the curves at three different titration speeds (0.173, 0.0184, and 0.0475 mole H^+/mole Al-min) superimpose quite well. This resultant curve may be said to describe a pseudo-equilibrium state as the measured pH values do not correspond with those derived from thermodynamic data especially in region B. Stol (2) observed deviations from the pseudo-equilibrium curve at titration speeds below 2.7×10^{-3} mole H^+/mole Al-min.

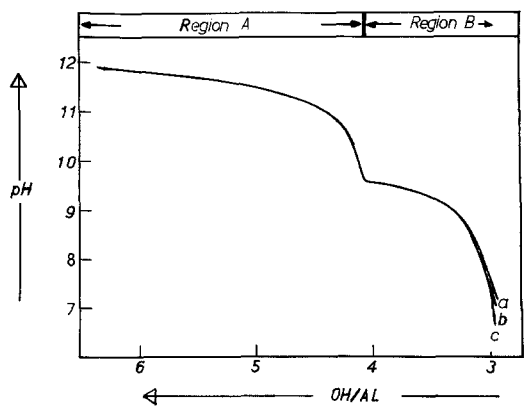

FIG. 1. Titration curves (pH vs OH/Al) at three different titration speeds: (a) 0.173 mole H^+/mole Al min; (b) 0.0814 mole H^+/mole Al min; (c) 0.0485 mole H^+/mole Al min. Total aluminate concentration is 4×10^{-3} M in all three experiments.

The same characteristic shape of the titration curves is also obtained when the total aluminate concentration is varied as is shown in Fig. 2. In this figure we plotted as ordinate the function $X = \text{pH} + p\text{Al}_T$ where we define $p\text{Al}_T$ as the negative logarithm of the total aluminate concentration. The choice of the function X is not altogether arbitrary but is based on the reasonable assumption that the anion Al(OH)_4^- is the predominating Al(III)-bearing species. Again we note the three titration curves (different $p\text{Al}_T$) to superimpose reasonably well.

In region A where no solid phase forms during the relatively fast titrations, we find on comparing experiments with different aluminate concentrations at the same OH/Al ratio the identity $\text{pH}_1 + p\text{Al}_{T,1} = \text{pH}_2 + p\text{Al}_{T,2}$ to be reasonably well obeyed. More surprising is the observation that this identity also seems to hold well in region B at the different titration speeds. This finding strongly suggests that during the titration pseudo-equilibrium is established as previously mentioned.

We attempted to synthesize a theoretical titration curve by postulating the following two "equilibrium" reactions:

$$\text{H}^+(\text{aq}) + \text{OH}^-(\text{aq}) \rightleftarrows \text{H}_2\text{O}(1); \quad K_W = 10^{-14} \qquad [1]$$

$$\text{H}^+(\text{aq}) + \text{Al(OH)}_4^-(\text{aq}) \rightleftarrows \text{Al(OH)}_3(\text{s}) + \text{H}_2\text{O}(1); \quad K_s = 8 \times 10^{-13} \qquad [2]$$

and making use of the Davies expression for calculating activity coefficients (17). The magnitude of K_s was chosen so as to give the best fit with the experimental curves. This calculated curve is also plotted in Fig. 2. The general features of the experimental curves are quite well reproduced by the postulated reaction scheme. A small but significant discrepancy between the theoretical and experimental curves is, however, evident in the transition from region A to B. We shall attempt to account for this deviation later on in the discussion section.

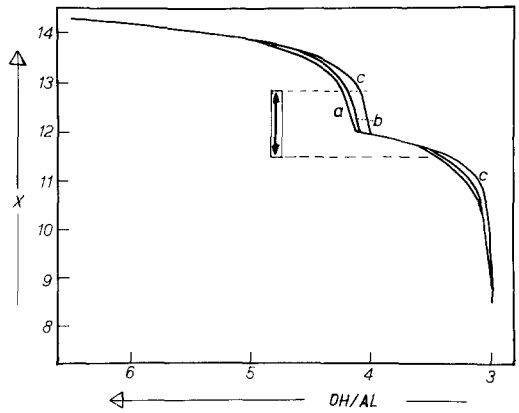

FIG. 2. Titration curves ($X(=\text{pH} + p\text{Al}_T)$ vs OH/Al) at different total aluminate concentrations: (curve a) $p\text{Al}_T = 3.0$; (curve b) $p\text{Al}_T = 2.4$ and 1.8; (curve c) calculated curve (see text). Titration speed 0.081 ± 0.01 mole H^+/mole Al min. Double arrow indicates region of supersaturation investigated in relaxation experiments.

Relaxation Curves at Constant pH

The relaxation studies were performed at different initial supersaturations where we define the supersaturation Π as

$$\Pi = \frac{a_{\text{Al(OH)}_4^-} \cdot a_{\text{H}^+}}{K_{sp}} \qquad [3]$$

where a_i is the activity of ionic species i in the supersaturated solution and K_{sp} is the solubility product of the precipitating phase. When more than one solid phase may precipitate (as is true in this study) the initial supersaturation cannot be characterized by a unique value. Since we are mainly interested in the effect of changing supersaturation, this problem is circumvented by introducing the function $X \equiv \text{pH} + p\text{Al}_T$ as an operational measure of the supersaturation. This parameter has the property that $d(p\Pi_j) = dX$ for all possible phases j involved and its value will decrease with increasing supersaturation. In the experimental program the supersaturation of any precipitating phase was fixed by specifying X and the chosen range of X values was dictated by some practical and experimental

requirements. Within the chosen supersaturation interval the pH must be a sensitive function of (small) changes in the OH/Al ratio. The time required for the appearance of the solid phase should be neither too short nor too long. In the former instance it would not be possible to follow the precipitation event and in the latter instance the accuracy of the measurements will suffer because of drift in the electrode potential. The range of experimental X values at fixed $p\mathrm{Al_T}$ is also indicated in Fig. 2.

Typical examples of the measured relaxation curves, α versus t, are given in Fig. 3. The parameter α measures the extent (or progress) of the precipitation reaction and is determined operationally from the expression

$$\alpha = \frac{\Delta H(t)}{C_{\mathrm{Al(T)}}} \qquad [4]$$

where $\Delta H(t)$ is the cumulative amount of acid added at time t to the system relaxing at constant pH with a constant amount of aluminum, $C_{\mathrm{Al(T)}}$.

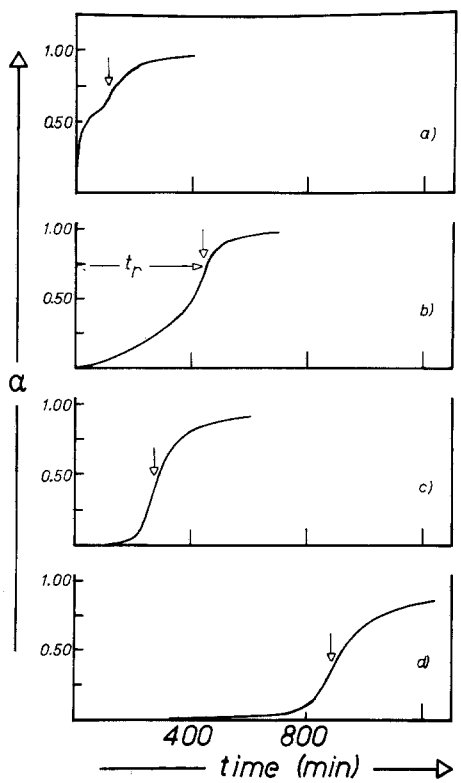

FIG. 3. Constant pH relaxation curves (α vs time (min)) at different initial supersaturations but constant $p\mathrm{Al_T} = 1.8$: (a) pH 10.15; (b) pH 10.45; (c) pH 10.85; (d) pH 11.05. Arrows point to location of relaxation time t_r (see text).

We notice three distinct types of relaxation curves depending on the magnitude of the initial supersaturation. At low supersaturations (Figs. 3c and d) a time lag precedes the uptake of acid. At relatively high supersaturations (Fig. 3a) two different stages in the relaxation process may be distinguished. In the first stage an immediate and fast acid uptake, which then slows down gradually, occurs. The second stage is characterized by a maximum in the relaxation rate ($d\alpha/dt$). At intermediate (initial) supersaturation levels (Fig. 3b) the acid uptake also starts immediately but at a much slower rate than at higher supersaturations. No second stage is noticeable and the maximum relaxation rate is seen to occur at higher α values than in either of the other two types of relaxation curve.

To characterize all relaxation curves we introduce the relaxation time t_r, an experimental parameter which is determined by the time taken for the relaxation rate to pass through a maximum (see Fig. 3). For relaxation curves at high supersaturations, t_r relates to the second stage (see Fig. 3a). In general the magnitude of t_r is seen to depend on the initial degree of supersaturation.

The relaxation curve in Fig. 3a corresponds to the highest supersaturation realizable in region A of the titration curve (Fig. 2). Constant pH relaxations in region B show very fast acid uptakes because of the establishment of pseudo-equilibrium referred to before. This fast uptake is then followed by a slower process. The two-stage relaxation noted in Fig. 3a is also conspicuous in the experiments in region B. In Fig. 4 we give examples of these relaxation curves as obtained at a total aluminate concentration of 4×10^{-3} M and an ionic strength of 0.15 M. The initial very rapid

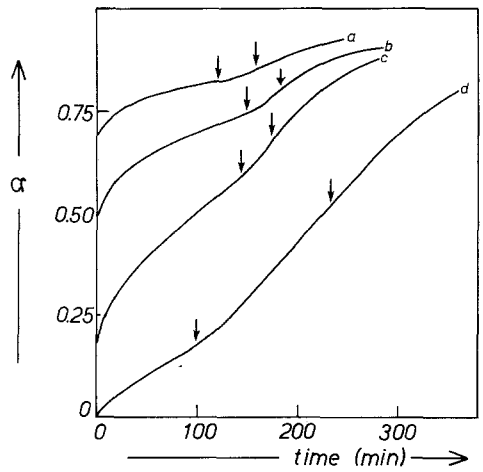

FIG. 4. Constant pH relaxation curves in region B show initial fast uptake of acid at constant pAl_T = 2.4: (a) pH 9.15; (b) pH 9.35; (c) pH 9.55; (d) pH 9.65; ↓ Indicates location of maximum uptake rate in second stage. ⇓ Point of transition between two stages.

acid uptake noticeable in curves a, b, and c is not apparent in curve d which is representative of the relaxation in that part of region A bordering on region B.

The same sequence of relaxation curves depicted in Fig. 3 is also observed at all other investigated aluminate concentrations. This is illustrated in Fig. 5 where relaxation curves at the same initial supersaturation (constant X) but different pAl_T values are compared. All curves in this figure show the same sequence of a fast initial uptake followed by a two-stage process where we note smaller t_r values at higher aluminate-concentrations.

Precipitation Sequence

The solid phase formed in the (fast) titration experiments was almost completely X-ray amorphous. Only faint bands of pseudo-boehmite could be detected. This observation depends on the titration speed, as Stol (2) was able to obtain bayerite in similar experiments at much lower titration rates. The first fast uptake of acid in the experiments described by curves a, b, and c in Fig. 4 corresponds actually to a fast titration into region B (Fig. 2) and indicates that initially there an amorphous phase also formed. In the following discussion the end of the first uptake (see Figs. 4a, b, c) is regarded as the starting point of the relaxation experiments.

In all experiments with two-stage relaxations, detailed IR and X-ray studies show mainly pseudo-boehmite, a gelatinous aluminumoxyhydroxide [AlO(OH)] to form during the first stage whereas crystalline bayerite, $Al(OH)_3$, precipitated in the second stage. In Fig. 6 the two types of X-ray spectra observed are given. Figure 6a displays the spectrum of a solid sample of only bayerite and in Fig. 6b the broad bands characteristic of pseudo-boehmite are seen superimposed on the bayerite diffraction pattern.

At low supersaturations (one stage relaxation) only bayerite could be detected and at intermediate supersaturations the fraction of pseudo-boehmite appeared to diminish in the end product with decreasing supersaturation.

Large differences in the specific surface of pseudo-boehmite and bayerite were also detected. In Table I a comparison is made between the BET surface areas of different samples. In experiments where pseudo-boehmite formed in measurable amounts the specific surface of solid samples is 200 to 300 m^2/g

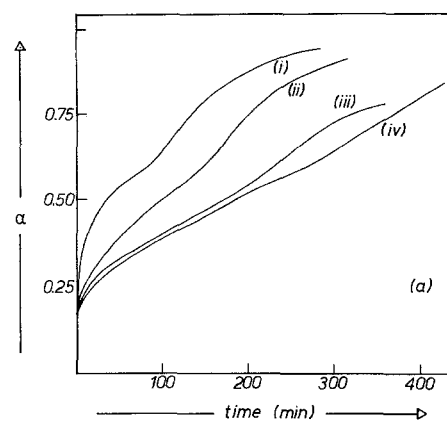

FIG. 5. Constant pH relaxation curves at varying pAl_T. X = 11.95; (i) pAl_T = 1.8; (ii) pAl_T = 2.4; (iii) pAl_T = 3.0; (iv) pAl_T = 3.3.

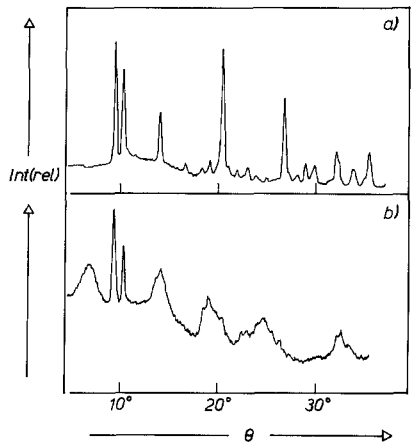

FIG. 6. X-Ray diffraction patterns of bayerite and pseudo-boehmite. (a) Bayerite; (b) mixture of bayerite and pseudo-boehmite.

whereas in experiments where only bayerite precipitated the specific surface is reduced by one to two decades. Noteworthy is that on aging a precipitate originally containing a mixture of the two solid phases in the mother liquor, only bayerite is detected afterward. This transformation is also accompanied by a drastic decrease in specific surface (see Table I).

Relaxation Time Curves

In Fig. 7 the relaxation time t_r, evaluated by the procedure described earlier, is plotted against the function $X(=\text{pH} + p\text{Al}_T)$ which is a measure of the initial supersaturation in a given relaxation experiment. Four series of experiments were carried out, at four different $p\text{Al}_T$ values but always at a constant ionic strength of 0.15 M by adding where necessary KNO_3 to the relaxing system. The supersaturation intervals wherein the three solid phases (amorphous, pseudo-boehmite, and bayerite) are formed are also indicated in Fig. 7.

A surprising feature of the t_r versus X plots is the well-developed maximum at intermediate supersaturations where both pseudo-boehmite and bayerite form. At high supersaturations (low X) the relaxation time tends to reach a plateau value independent of X whereas at low supersaturations the relaxation time rises steeply to reach a very high (infinite) value. The effect of increasing the $p\text{Al}_T$ is seen as a slight lowering of t_r at the same X (identical supersaturation).

At a total aluminate concentration of 4×10^{-3} M pH stat experiments were also done at ionic strengths of 0.026 M (no added KNO_3) and 0.51 M in addition to 0.15 M. Only minor differences in the observed relaxation times and relaxation rates were noted. The precipitation sequence and the relaxation pattern remained unaffected by these changes in ionic strength.

Constant pH Seed Experiments

A number of relaxation experiments were run in which 10 g of gibbsite (Merck, BET surface area 0.3 m^2/g) were introduced just before reaching the desired supersaturation. The total aluminate concentration in this series of experiments were 4×10^{-3} and 4×10^{-4} M and the initial supersaturations were on the low side. The experimental relaxation curves (α versus t) are displayed in Fig. 8. Conspicuous is the absence of a lag time which is so characteristic of the unseeded experiments

TABLE I

BET-Surfaces under Various Experimental Conditions

$p\text{Al}_T$	pH	α	Phase[a]	BET (m^2/g)
1.8	10.15	0.95	ps-B + Bay	127 (14)[b]
	10.45	0.95	Bay + Ps-B	58 (2)
	11.05	0.9	Bay	3
2.1	9.85	0.5	ps-B	254
		0.7	ps-B + −Bay	220
		0.95	ps-B + Bay	168
2.4	9.55	0.95	ps-B + Bay	209 (15)
	9.65	0.95	ps-B + Bay	156
	9.75	0.90	ps-B + Bay	143
	9.85	0.95	ps-B + Bay	78
	9.95	0.95	ps-B + Bay	5
	10.15	0.90	Bay	5

[a] ps-B, pseudo-boehmite; Bay, bayerite.

[b] Specific surfaces in parentheses obtained after aging for about 3 months.

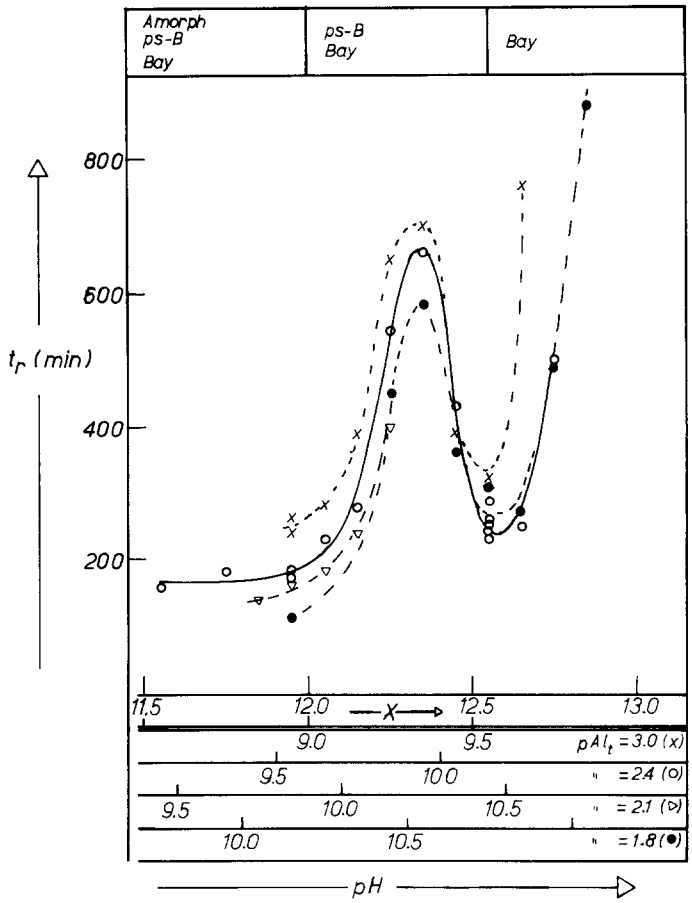

FIG. 7. Relaxation time as a function of X and pH at different pAl_T: ×, pAl_T = 3.0; ○, pAl_T = 2.4; △, pAl_T = 2.1; ●, pAl_T = 1.8.

(Figs. 3c and d) at the same low initial supersaturations. Simple calculations show that the increase in total amount of solid phase during the relaxation is maximally 10% for $C_{Al(T)} = 4 \times 10^{-3}$ M and only 1% for $C_{Al(T)} = 4 \times 10^{-4}$ M.

DISCUSSION

Analysis of the Titration Curves

We have shown that the basic features of the "pseudo-equilibrium" titration curves in Figs. 1 and 2 may be reproduced by calculation based on a simple reaction model. One of the reactions in this model, namely reaction [2], describes the near instantaneous formation of an amorphous solid. By choosing for this reaction pK_s = 12.1 the best fit between the model and experiment was obtained. This value of the "equilibrium constant" is slightly smaller than values quoted in the literature for freshly prepared aluminum hydroxide precipitates. Brosset (18), for example, found pK_s = 12.5 ± 0.2 at 40°C in solutions 2 M in perchlorate ions. Hem and Roberson (19) report a value of pK_s = 12.7 for precipitates aged for 1 day. The experimental pK values clearly depend on the method of precipitation and on the aging time. We observed the appearance of different crystalline phases within one day from the start of pH stat experiments. The pK_s value reported above is, we believe,

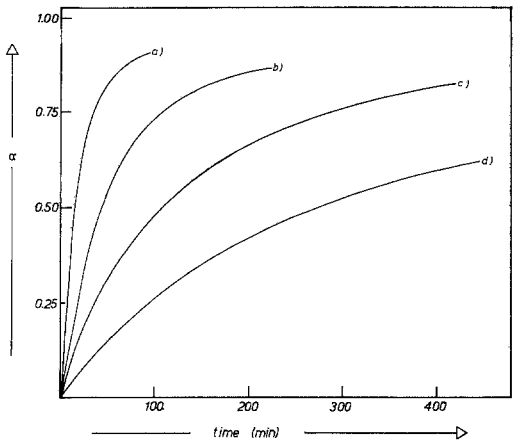

FIG. 8. Constant pH relaxation curves in seed experiments at constant $pAl_T = 2.4$ and $I = 0.15$: (a) pH 10.35; (b) pH 10.65; (c) pH 10.95; (d) pH 11.25.

a reasonable estimate of the formation constant of the amorphous solid as produced under the experimental conditions in our study.

Up till now we have assumed the aluminate anion $[Al(OH)_4^-]$ to be the only soluble Al(III)-bearing species in alkaline solutions. Now the previously mentioned small but significant deviation between the theoretical and experimental titration curves (see Fig. 2) may be shown to imply a slightly larger number of OH^- ligands to be bonded to one Al atom than the four ligands in the aluminate ion. Calculation shows the bonding ratio to be 4.07 ± 0.03. A similar discrepancy was already noted by Brosset (18, 20) although he did not comment on this. In their EMF studies of aluminate solutions with a special electrode sensitive to the aluminum/aluminate couple, Plumb and Swaine (21) also noted this discrepancy. They tried to explain their findings by postulating the presence of chains of the type $\{(OH)_2[Al(OH)_4^-]_n\}^{-(n+2)}$. On the assumption that all the aluminum is present in these chains these authors arrive at chains with $n = 40$–100. In view of numerous independent measurements (4–6) which clearly indicate the monomeric species $Al(OH)_4^-$ and, at high concentrations, probably also AlO_2^- to be the dominating species, the assumption made by Plumb and Swaine must be an exaggeration. It is however possible that a small fraction of low polymeric chains may be present in solution. A similar suggestion was also made by Eremin *et al.* (6).

Precipitation Sequence and Relaxation Times

The formation of bayerite was observed at all the investigated supersaturations. At high supersaturations its appearance was preceded by the formation of pseudo-boehmite and in region B (see Fig. 1) of the titration curve an X ray amorphous phase was noted to form immediately. On the basis of our pH-stat relaxation studies we are able to distinguish the following precipitation sequences in three different supersaturation regions:

I.	amorphous-pseudo-boehmite-bayerite;	$X < 12$
II.	pseudo-boehmite-bayerite;	$12 < X < 12.55$
III.	bayerite;	$X > 12.55$.

The precipitation sequence at high supersaturations (small $X = pH + pAl_T$) may be compared with available thermodynamic data on the relative stability of the solid modifications of $Al(OH)_3$. From Table II which lists experimentally observed solubility products the following order (despite the scatter in the reported values) for increasing thermodynamic stability of the various modifications is indicated:

amorphous ≈ pseudo-boehmite
< bayerite < gibbsite.

This sequence is also the precipitation sequence derived from our kinetic studies except

TABLE II

Solubility Products for Different Solid Modifications of Aluminum Hydroxide[a]

Substance	pK_s	Ref.
Fresh precipitate/ amorphous/ pseudoboehmite	12.50 (40°C)	18
	12.62 (20°C)	42
	12.70	19
Bayerite	13.84	43
	13.96	19
	14.52	46
	14.82	44
Gibbsite	14.57	43
	15.26	47
	15.27	44
	15.30	45

[a] Temperature is 25°C unless indicated otherwise.

that we could not detect the presence of gibbsite. This phase might have been present in very small amounts. In a second publication we shall report on experimental conditions (high temperatures and/or high pH) where gibbsite has been observed to form in considerable amounts.

We may conclude that at room temperature and at high supersaturations where the solution is supersaturated with respect to all possible solid modifications, the thermodynamically less stable phase (amorphous or pseudoboehmite) precipitates before the more stable phase (bayerite). This observation confirms the well-known "Law of Stages" formulated by Ostwald in 1897 which states that a system will approach equilibrium through a sequence of high-energy states (13).

As precipitation sequences are established under nonequilibrium (kinetic) conditions it is to be questioned whether the results can be satisfactorily accounted for by a simple thermodynamic rule. Over the last 50 years a kinetic approach with as its basis classical nucleation theory has been developed to explain and predict precipitation sequences. It may be referred to as the "kinetic rule of stages." Stranski and Totomanov (22) introduced this approach in 1933. Gutzow and Toschev (23) extended this approach by taking into account nonsteady nucleation and focusing attention on the importance of induction times. Feenstra (14) elaborated on the treatment of Gutzow and Toschev and clearly stated the limitation of the thermodynamic Rule of Ostwald.

In order to appreciate the significance of this kinetic rule in our own studies we shall give a brief review of the fundamentals on which it is based. According to classical nucleation theory (24) the steady-state rate of homogeneous nucleation is given by the expression

$$J = A \exp(-\Delta G_c/kT) \qquad [5]$$

where the exponential term determines the probability that by a fluctuation in the supersaturated solution, a critical nucleus of the new phase will form. The free energy difference ΔG_c measures the reversible work required for formation of the critical nucleus at constant pressure and temperature. It is a sensitive function of the interfacial tension σ and the supersaturation Π,

$$\Delta G_c \propto \frac{\sigma^{n+1}}{(\ln \Pi)^n} \qquad [6]$$

where $n = 2$ for the formation of a three-dimensional nucleus and $n = 1$ for the formation of a two-dimensional critical nucleus. In the latter case the interfacial tension in Eq. [6] should be replaced by the line tension γ but as a first approximation we may write $\gamma = \sigma v^{1/3}$ where v is the average molecular volume of the precipitating phase. The pre-exponential factor A is derived from a suitable model for the collision mechanism by which the critical nucleus is supposed to evolve from monomeric species. From Eqs. [5] and [6] we may conclude that

$$J_X > J_Y \qquad [7]$$

provided $(\Delta G_c)_X < (\Delta G_c)_Y$ and/or $A_X > A_Y$ where X and Y refer to two solid modifications both of which may precipitate.

Quite often it takes a finite time before reaching a steady-state nucleation rate. This nonstationary period of nucleation is characterized by the so-called induction time τ for which we may write the general expression

$$\tau = B \exp(+\Delta G_c'/kT) \qquad [8]$$

where $\Delta G_c'$ is the free energy of formation of a two-dimensional (surface) critical nucleus and the pre-exponential factor is determined by the details of the mechanism of growth of this nucleus. As pointed out by Toschev (25) and Feenstra (14) the lag times observed in nucleation experiments in liquid are almost always related to nonstationary phenomena and may be evaluated by an elaboration of Eq. [8]. A delay time may, however, be measured experimentally even though it is quite likely that a stationary state has been established. This "induction" time is determined solely by the sensitivity of the experimental technique used for detecting changes in the supersaturated state due to the occurrence of random nucleation events. It is defined by

$$\langle t \rangle = \frac{1}{J} = A^{-1} \exp(\Delta G_c/kT) \qquad [9]$$

where ΔG_c refers to a three-dimensional critical nucleus. This delay time $\langle t \rangle$ provides information on the size of the steady-state flux whereas τ is more fundamentally related to the decay of the non-steady state.

As pointed out by Feenstra (14) both J and τ must be considered in an attempt to explain or predict a given precipitation sequence in supersaturated liquid systems. For example, when an amorphous (X) and a crystalline modification (Y) may both precipitate ($\Pi(Y) > \Pi(X) > 1$) in a solution of given composition the former may still be favored ($J_X > J_Y$; $\tau_X < \tau_Y$) for two kinetic reasons. Because of the more disordered structure of X its surface will be quite rough and the chance of a monomer sticking to the surface will be greater. The pre-exponential factors in Eqs. [5] and [8] will then favor X. In the extreme case, all the surface sites will be available as nucleation centers and growth sites and there will be no need for a two-dimensional nucleus to form. Growth of the critical nucleus on Y will be restricted by the availability of growth sites (adjacent to the surface nucleus). The higher structural order of this solid modification may also be reflected in a higher activation energy barrier for nucleation provided $\sigma_Y > \sigma_X$ (see Eq. [6]). This suggestion is supported by the interesting correlation between the interfacial tension and solubility for inorganic salts observed by Nielsen and Söhnel (7, 26). These investigators concluded from nucleation experiments with salts of very different solubility that a lower solubility is connected with a higher σ value. We may therefore conclude that there will be a supersaturation range where the formation of the thermodynamically least stable amorphous phase will be favored because its induction time will be smaller and its nucleation frequency will be larger than that of the crystalline phase. The prediction of a precipitation sequence involving more than one crystalline modification will not be as straightforward, especially, because the relative magnitudes of the pre-exponential factors in the expressions for J and τ are not so easily established by qualitative reasoning.

The three experimental precipitation sequences observed in our study may be readily explained by the kinetic arguments just presented. Some additional comments on the precipitation sequence, pseudo-boehmite $\rightarrow$ bayerite should be made. According to Lippens (27) pseudo-boehmite may be regarded as a partially hydrated boehmite where the excess water is bound by strong hydrogen bonds between layers. The extension of the lattice by the extra water is irregular. The separate boehmite layers are stacked imperfectly and this behavior explains both the extension of the c axis with increasing water content and the broadening of the diffraction peaks (Fig. 6b). Pseudo-boehmite therefore has a less ordered structure than bayerite. This is also supported by the high specific surface (200–300 m^2/g) and the spongy appearance in the elec-

tron microscope of pseudo-boehmite. Based on these facts one would expect pseudo-boehmite to nucleate and grow more readily than bayerite.

Although we are able to give a satisfactory qualitative explanation for the observed precipitation sequences, the interpretation of the relaxation curves, t_r versus X, in Fig. 7 is not as simple. It is tempting to equate the measured relaxation times to the theoretical induction times τ and refer this to the formation of bayerite. The conventional nucleation theory (see also Eqs. [5] and [8]), predicts a monotonic rise in the induction time with decreasing supersaturation. The two extrema in the experimental curves (Fig. 7) are, however, at variance with theoretical prediction. It is possible that the extrema are artifacts introduced by incorrect evaluation of the supersaturation. As can be seen from Fig. 4, at high initial supersaturations (small values of X) up to 80% of the available aluminate is consumed in the prior formation of amorphous and pseudo-boehmite. Under these conditions the actual supersaturation at which bayerite forms will be lower (X larger) than indicated in Fig. 7. On making this correction the experimental points on the extreme left hand-side of the graphical plots are indeed shifted horizontally toward the right but not so as to eliminate the maximum in the curves. This failure to remove the extrema is largely due to the experimental fact that in the supersaturation region where the maximum falls bayerite is overwhelmingly present in the precipitate. The positions of the extrema are therefore fixed and the simple explanation of the relaxation time curves must be discarded although it should account for the extreme right-hand branch of the curve.

Now the change in supersaturation at fixed total aluminate concentration has been achieved by a change in pH and instead of choosing as abscissa the supersaturation (X) we may elect the pH (see Fig. 7). The extrema are certainly not eliminated by this substitution, but it focuses attention on the role of the pH. It is conceivable that aside from its role in fixing the supersaturation, the pH also fulfills a more specific function. This conclusion is not surprising because it is a well-established fact that the electrical double layer around oxide and hydroxide solids is established by adsorption of the so-called potential-determining ions, H^+ and OH^-. On changing the pH, the sign and magnitude of the surface charge density and thus the interfacial tension will be altered.

If both σ and Π were to decrease with increasing pH then the induction time τ may either increase (due to a decrease in Π) or decrease (due to a lowering of σ) within a given range of pH (see Eqs. [6] and [8]). A maximum in the τ versus pH curve will then be obtained if (a) in the low pH range the supersaturation is lowered more strongly than the interfacial tension and (b) in the high pH range the reverse is true. The minimum in the induction time versus pH curve which lies on the high pH side of the maximum is then simply accounted for. Regardless of what happens to σ, when the solution is nearsaturated ($\Pi \approx 1$) the induction time must increase again. This interpretation of the extrema in the τ versus pH curves will account qualitatively for the experimental measurements in our system. As the point-of-zero-charge (pzc) for $Al(OH)_3$ is known to fall in the pH range 9 to 9.2 (28) one would expect the interfacial tension to be decreased under the conditions maintained in our experiments. We must however demonstrate that the theoretical prediction is in reasonable quantitative agreement with experiment. In order to make this test for consistency we need expressions for τ and σ as functions of pH.

It is reasonable to relate the induction time for crystalline bayerite to a model requiring the formation of a two-dimensional nucleus on the surface of the growing critical nucleus. Starting with this model Gindt and Kern (29) and Feenstra (14) derived an expression for the pre-exponential factor in Eq. [8] to arrive at the following relation:

$$\tau = C_1\left(\frac{\sigma}{\ln \Pi}\right)^3 \exp\left(\frac{C_2\sigma^2}{\ln \Pi}\right) \qquad [10]$$

where C_1 is essentially a constant at a given temperature and includes an activation energy to be referred to later on, $C_2 = 4v^{4/3}/(kT)^2$ assuming a square 2-D critical nucleus.

Recently Stol and De Bruyn (30) calculated the change in interfacial tension due to adsorption of the potential-determining ions (H^+, OH^-) at the oxide/solution interface as a function of the parameter, $\Delta pH = pH - pH_{pzc}$ by introducing a simple model of the electrical double layer. For the sake of simplicity we approximate the dependence of σ on pH (or ΔpH) by the expression

$$\sigma = \sigma_0 - b(\Delta pH)^2 \qquad [11]$$

where σ_0 is the (maximum) interfacial tension at the point-of-zero-charge (located by pH_{pzc}) and b is a constant. This parabolic expression describes the variation in σ found by Stol and De Bruyn sufficiently accurately for our purpose.

By combining Eqs. [10] and [11] graphical plots of $\ln(\tau/C_1)$ versus pH for different values of the "adsorption" parameters σ_0/b may be constructed. Examples of such plots are given in Fig. 9. In making the calculations leading to these plots we chose pK_{sp}(bayerite) = 14.5, $pH_{pzc} = 9$, $\sigma_0 = 100$ mN/m, $T = 298°K$, and $C_{Al(T)} = 0.4\ M$. The choice of these physical and chemical quantities is not too arbitrary but is based on reasonable estimates for the bayerite system. The high value for the total aluminate concentration enables one to cover quite a wide range of ΔpH.

We note from Fig. 9 that depending on the value chosen for σ_0/b three different types of curves are obtained. At high σ_0/b values (relatively small changes in σ), $\ln(\tau/C_1)$ increases steadily with increasing pH. At low σ_0/b values (large changes in σ), $\ln(\tau/C_1)$ passes through a maximum and then goes to minus infinity. At intermediate values of σ_0/b both a maximum and minimum are obtained. This special situation arises when $\ln \Pi$ becomes zero ($\Pi = 1$) at a pH where a substantial lowering of the interfacial tension has also occurred.

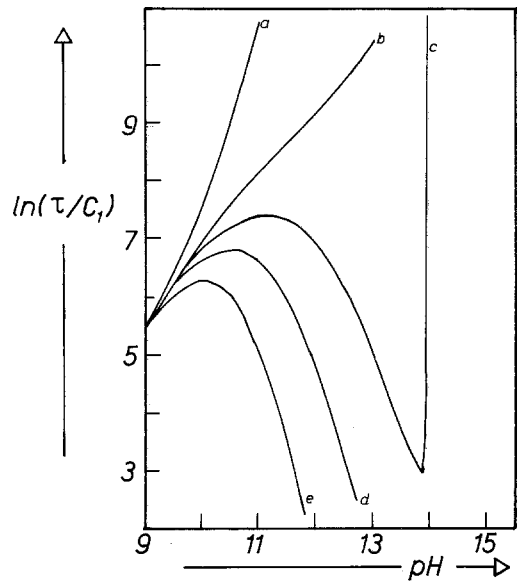

FIG. 9. Calculated curves of $\ln(\tau/C_1)$ vs pH. (a) $\sigma_0/b = \infty$; (b) $\sigma_0/b = 33$; (c) $\sigma_0/b = 25$; (d) $\sigma_0/b = 20$; (e) $\sigma_0/b = 14$.

We have thus demonstrated that extrema in the variation of τ with pH may be accounted for (semi-)quantitatively by a concomitant decrease in both σ and Π with increasing pH *provided* a significant decrease in the interfacial tension is realized within the chosen range of ΔpH. When we compare the theoretical analysis (Fig. 9) with the experimental data (Fig. 7) we note that in the latter case the extrema lie closer to the pH_{pzc}($\Delta pH \approx 1$–2) than in the former ($\Delta pH \approx 3$ to 4). In the experiment moreover the maximum and minimum are separated by only 0.2 to 0.3 pH units. When we apply the theoretically derived condition for two extrema in the τ versus pH curves to explain the observed location of the experimental extrema unrealistic values for the solubility product, σ_0 and b are, however, required. Furthermore, according to the theory the location of the maximum at higher values of $C_{Al(T)}$ should shift to lower pH values, a result which is opposite to that found in the experiment (see Fig. 7). Theory also predicts

the minimum to disappear at specific values of the total aluminate concentrations.

We must therefore conclude that the dual role of pH in decreasing the interfacial tension and the supersaturation cannot explain the behavior of the relaxation time curves under the chosen experimental conditions. This conclusion does not rule out the validity of this theoretical approach in explaining relaxation time–pH curves. It is conceivable that studies at higher $p\mathrm{Al}_T$ values than those chosen in this investigation may yield results consistent with theory. Such studies are in progress. An added feature of the analysis of induction times is the possibility of obtaining absolute interfacial tensions for solid/liquid systems.

The preceding analyses have made it clear that the relaxation time as measured experimentally cannot at all the supersaturations be equated to an induction time characteristic of the nucleation of bayerite. The same conclusion is reached when one considers the relaxation curves displayed in Fig. 3. Although the two curves at low supersaturation (Figs. 3c and d) may be made to superimpose by a simple translation along the time axis, this is not possible for the relaxation curve of Fig. 3b and certainly not for the curve in Fig. 3a. Obviously the relaxation processes at high, intermediate, and low supersaturations which yield three distinct precipitation sequences (I, II, and III) cannot be described by a single relaxation time parameter, such as $'\tau$, but must relate to different combinations of elementary kinetic steps. To find a satisfactory explanation of the t_r versus pH curves in Fig. 7 we divide these curves into three regions I, II, and III where the boundaries are approximately located by the X values which separate the three precipitation sequences (see also Fig. 7). We shall point out that by postulating certain kinetic conditions (based on the theories of nucleation and growth) to be fulfilled, the behavior of the experimental t_r versus X (or pH) curves in each region will be clarified. We consider now briefly each region separately in the order III, I, II.

Region III

In this region with as lower boundary $X > 12.55$ the only phase to nucleate and grow is bayerite. The nucleation flux of pseudoboehmite J_{pb} is zero either because the solution is saturated or even unsaturated with respect to this phase or because the supersaturation level is below a critical value for nucleation. The observed decrease in t_r with decreasing pH (increasing X) is simply explained by the effect of supersaturation on the induction time τ for the formation of bayerite according to Eq. [8].

Region I

In this region, located by $X < 12$, relatively large amounts of amorphous and pseudoboehmite form first. The formation of bayerite is postponed to a time when the supersaturation has dropped considerably. This delay time is measured by the value of t_r. We also note that bayerite forms immediately when this supersaturation is reached. No lag time in the relaxation behavior so characteristic of region III (Figs. 3c and d) is evident (see Fig. 3a). It is also interesting to note that the actual supersaturation at which bayerite forms in this region is practically independent of the initial supersaturation value.

These experimental observations form the basis for the following two postulates which in turn explain the behavior of t_r versus X(pH) curves: (a) $J_{pb} \gg J_b$ where J_i is the homogeneous (steady-state) nucleation rate of pseudoboehmite (pb) or bayerite (b). (b) Bayerite forms by heterogeneous nucleation on the surface of previously precipitated pseudoboehmite. Additional arguments in favor of postulate (a) have already been presented when we discussed the application of Eq. [7] to explain the observed precipitation sequence, pseudo-boehmite $\rightarrow$ bayerite. Postulate (b) follows from the observed absence of a lag time (i.e., $\tau = 0$) in the formation of bayerite after precipitation of pseudo-boehmite and the amorphous phase. The observed relaxation

time in this region simply measures the delay in the rapid heterogeneous nucleation of bayerite on pseudo-boehmite particles.

Region II

In this region, of which the extent is determined by the condition $12 < X < 12.55$, bayerite is the most abundant solid phase but varying small amounts of pseudo-boehmite are also present. The observed change in t_r which also includes the appearance of a maximum is therefore probably related to influence of the pseudo-boehmite on the induction time for bayerite. To account for the shape of the $t_r - X$ curve we introduce two postulates: (a) Homogeneous nucleation and growth of bayerite is retarded by heterogeneous nucleation of pseudo-boehmite on bayerite surfaces. (b) $dJ_{\text{homo(b)}}/d\Pi > dJ_{\text{hetero(pb)}}/d\Pi > 0$, the change in the homogeneous rate of nucleation of bayerite with increasing supersaturation is greater than the change in the heterogeneous nucleation rate of pseudo-boehmite with increasing II. Postulate (a) is in accord with the slow rise in the α versus t curve in Fig. 3b and will account for the unexpected rise in t_r when moving along the experimental curve from region III into region II (see Fig. 7). A measure of the retardation will be provided by the fraction of pseudo-boehmite per unit surface of bayerite. This postulate may also apply to region I and provide an additional argument in favor of the delayed formation of bayerite. Postulate (b) is needed to account for the observed maximum.

The experimental results summarized in Fig. 10 provide additional support for these postulates. Three constant pH relaxation experiments were performed with the initial conditions ($p\text{Al}_T = 2.4$, pH = 10.15) at the minimum of the t_r versus pH curve (see Fig. 7). In one experiment the relaxation was allowed to proceed undisturbed at pH = 10.15. In a second experiment after reaching $\alpha = 0.2$ the pH was suddenly changed to pH = 9.95 (a value corresponding to the maximum in the t_r versus pH curve at $p\text{Al}_T = 2.4$) and the relaxation was then continued at this pH. The same jump in pH was introduced in the third experiment but at $\alpha = 0.7$. From Fig. 10 we note that the relaxation rate is decreased when the pH change is made at $\alpha = 0.2$ but is increased at $\alpha = 0.7$. It may be shown that in the second experiment after changing the pH at $\alpha = 0.2$ the supersaturation of the system places it in region II where pseudo-boehmite retards bayerite formation. In the third experiment the system finds itself in region III even after changing the pH because the supersaturation immediately before this change was lowered much more than in experiment two ($\alpha = 0.7 > \alpha = 0.2$). The retardation effect of pseudo-boehmite has been eliminated and the system will relax faster than in the undisturbed first experiment.

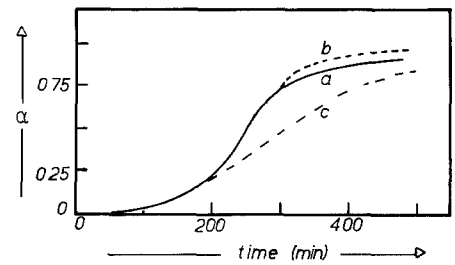

FIG. 10. Illustrating the effect of changing pH during relaxation. (a) Constant pH relaxation at $p\text{Al}_T = 2.4$ and pH = 10.15; (b) changing pH to 9.95 at $\alpha = 0.7$; (c) changing pH to 9.95 at $\alpha = 0.2$.

In conclusion we note that if the boundary separating regions II and III were to be fixed by the solubility of pseudo-boehmite then one finds by calculation that $pK_s = 12.7 \pm 0.05$ for this solid phase. This value is seen to be in good agreement with estimates derived from different experimental observations (see Table II).

Growth Kinetics of Bayerite

(1) Kinetic analysis of relaxation curves (α vs t). Information about the growth of bayerite may be obtained from the seeded and unseeded experiments at low supersaturations.

We noted that additional amount of solid phase formed during the relaxation in seed experiments was always small compared to the amount of seed crystals. If we now suppose that primary and secondary nucleation effects are negligible in these experiments then this would imply that the total surface area remained essentially constant throughout the relaxation process. On treating the relaxation as a heterogeneous chemical reaction, we may then write at constant pH

$$\frac{d\alpha}{dt} = k'_{r,h}[1 - \alpha(t)]^m \qquad [12]$$

where

$$1 - \alpha(t) = \frac{C_{Al(T)} - \Delta H(t)}{C_{Al(T)}} \qquad [13]$$

is a normalized aluminate concentration at time t and $k'_{r,h}$ is a pseudo-heterogeneous reaction rate constant. The reaction order m with respect to the aluminate concentration may then be evaluated by plotting the experimental results (Fig. 8) in the manner shown in Fig. 11.

We note that all the experimental results yield straight lines when plotted as shown in Fig. 11 with a slope (m) of 2.0 ± 0.05. The reaction rate is thus of order two in the aluminate concentration. Deviations from a straight line behavior are noticed at small α values and become more marked the lower the pH (the higher the supersaturation). The order of the growth reaction with respect to $[H^+]$ may be obtained by plotting the intercepts of the straightlines on the ordinate axis (Fig. 11) against pH as is shown in the insert on Fig. 11. An order of 1.7 ± 0.1 is thus obtained.

The second order dependence on the aluminate concentration is also obtained (as it

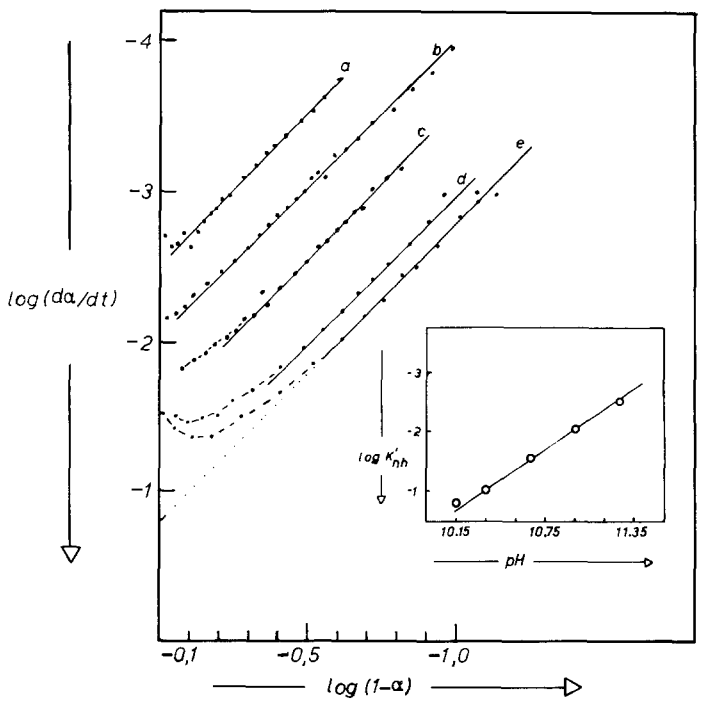

FIG. 11. Plots of log ($d\alpha/dt$) vs log ($1 - \alpha$) (according to Eq. [12] in text) at various pHs and identical pAl_T = 2.4 for seed experiments: (a) pH 11.25; (b) pH 10.95; (c) pH 10.65; (d) pH 10.35; (e) pH 10.15. Insert log $k'_{r,h}$ (see Eq. [12]) vs pH.

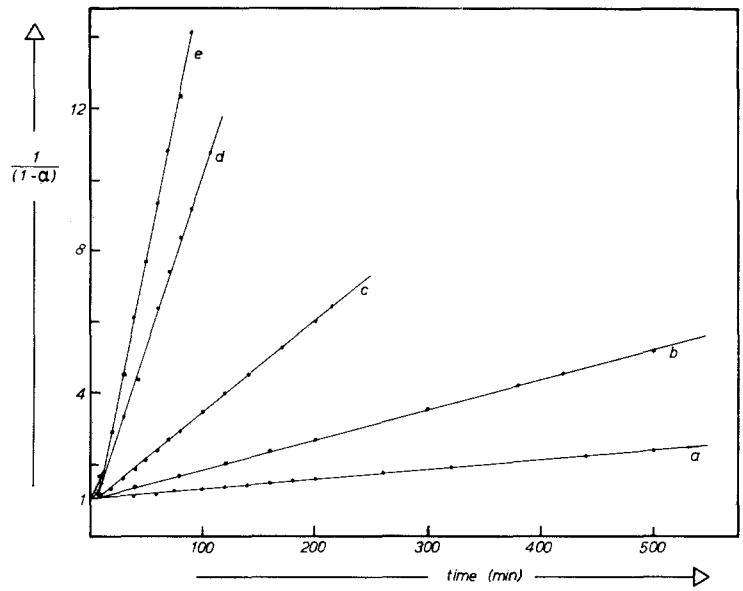

FIG. 12. Plots of reciprocal normalized aluminate-concentration ($1/(1 - \alpha)$) vs time at various pHs and identical $p\mathrm{Al_T} = 2.4$ for seed experiments: (a) pH 11.25; (b) pH 10.95; (c) pH 10.65; (d) pH 10.35; (e) pH 10.15.

should) by plotting $[1 - \alpha(t)]^{-1}$ versus t as is demonstrated in Fig. 12. The slopes of these straightlines equal $k'_{r,h}$ at a given pH. The failure of the straightlines to meet in one point on the ordinate axis again reflects deviations at low α-values from the postulated behavior (Eq. [12]). Figure 12 makes clear, however, that these deviations are restricted to the first few minutes of the relaxation.

Two additional comments need to be made regarding this kinetic analysis of the seed experiments. First, the data used to test Eq. [12] in Fig. 11 were provided by seed experiments performed at supersaturations falling in region III. Studies with seeding at higher supersaturations give more serious deviations from straightline behavior when the results are plotted as in Fig. 11. This observation must be attributed to the presence of pseudoboehmite. Second, we must inquire whether bayerite and not gibbsite is being formed on the surface of the gibbsite seeds. In the experiments with $C_{\mathrm{Al(T)}} = 4 \times 10^{-3}$ M approximately 10% of the final reaction product represents newly formed solid. X-Ray and IR investigations of the end product revealed the presence of bayerite in addition to the major component (gibbsite). Bayerite must therefore have grown on the gibbsite seeds. Apparently under the experimental conditions used, the thermodynamically more stable crystalline modification does not form.

A kinetic analysis of the relaxation curves in the unseeded experiments is complicated in the early stages of relaxation by the simultaneous formation of new surface by nucleation events and the increase in surface by growth of critical nuclei. At a given time at low α the total surface area will therefore be a complex function of α. The amount of new surface created would be directly proportional to α, whereas the surface area of a growing particle will be proportional to $\alpha^{2/3}$, if the shape of these particles is assumed not to alter during the growth process.

In the early stages of relaxation in unseeded experiments more surface will probably be generated through nucleation than will be enlarged by growth. Under these conditions the observed changes in the rate of acid uptake

$(d\alpha/dt)$ would reflect changes in nucleation rates due to a lowering of the supersaturation. Such changes will have a different dependence on aluminate concentration as the nucleation rate is a much more sensitive function of solute concentration than is crystal growth.

To arrive at an expression for the growth rate in these experiments we modify Eq. [12] to read

$$\frac{d\alpha}{dt} = C(\text{pH})[\alpha(t)]^{2/3}[1 - \alpha(t)]^m \quad [14]$$

where $[\alpha(t)]^{2/3}$ determines the cumulative amount of surface formed due to the growth of a constant number of particles. The pseudo-rate constant C will be a function of pH. This expression is of course expected to apply to a more restricted range of α values than in the case of seed experiments. A plot of log $\{(d\alpha/dt)[\alpha(t)]^{-2/3}\}$ against log $(1 - \alpha(t))$ should yield straightlines when only growth is responsible for the observed relaxation behavior. Such plots are given in Fig. 13 for a series of constant pH relaxations with initial supersaturations in region III (see Fig. 7). A straightline behavior as predicted by Eq. [14] is seen to hold for $0.5 \leqslant \alpha \leqslant 0.9$. For $\alpha < 0.5$ the growth of bayerite will be masked by the occurrence of nucleation which might even dominate at very low α values.

The results of the kinetic analysis of seed experiments according to Eq. [12] and unseeded experiments according to Eq. [14] are summarized in Table III, where $m(n)$ refers to the order of the growth reaction with respect to the aluminate (hydrogen ion) concentration.

(2) Growth models and the precipitation kinetics. From the kinetic analysis of the relaxation experiments at low supersaturations we derived a second order dependence of the growth rate on the aluminate concentration and an order between 1.5 and 1.8 for the hydrogen ion concentration. The order with re-

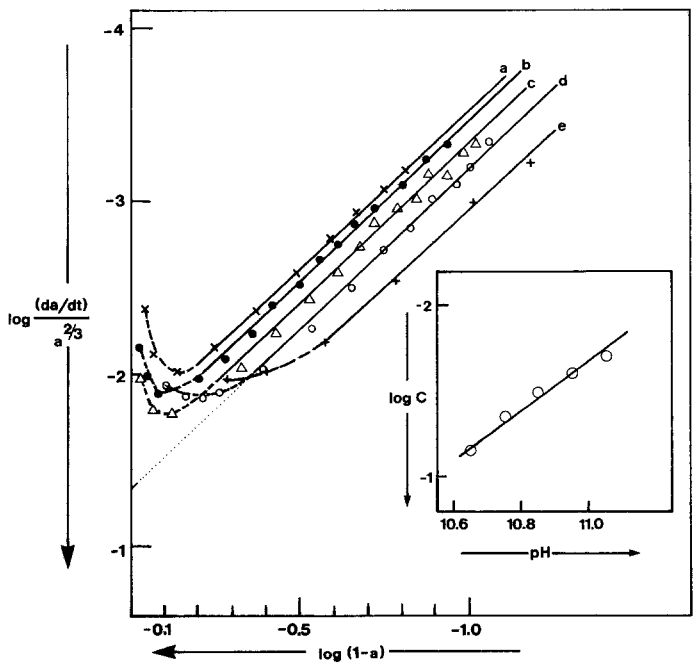

FIG. 13. Plots of log $((1/\alpha^{2/3})d\alpha/dt)$ vs log $(1 - \alpha)$ according to Eq. [14] for unseeded experiments at various pHs but constant $p\text{Al}_T = 1.8$: (a) pH 11.05; (b) pH 10.95; (c) pH 10.85; (d) pH 10.75; (e) pH 10.65. Insert log C (see Eq. [14]) vs pH.

TABLE III

Results of Kinetic Analysis of Relaxation Studies[a]

Experiment	m	n	pAl_T	pH range	I
With seeds	2.0 ± 0.05	1.7 ± 0.1	2.4	10.15–11.25	0.15 (M)
	2.0 ± 0.10	1.7 ± 0.1	3.4	9.15–10.45	0.15
Unseeded	2.0 ± 0.1	1.4 ± 0.3	1.8	10.66–11.05	0.15
	1.9 ± 0.2	1.7 ± 0.4	2.4	10.15–10.35	0.15

[a] I = ionic strength; pAl_T initial aluminate concentration ($-\log c_{Al(T)}$); pH range gives interval in which reaction order has been evaluated based on the following expressions. $d\alpha/dt = k'_{r,h} \cdot [1 - \alpha]^m \cdot [H^+]^n$ (seed) and $d\alpha/dt = C \cdot \alpha^{2/3} \cdot (1 - \alpha)^m \cdot [H^+]^n$ (unseeded).

spect to H^+ has been determined indirectly and with less accuracy than that with respect to aluminate. The higher order of 1.8 is obtained in the seed experiments and is a more reliable estimate because only small, if any, changes in total surface are to be expected. We may go one step further and assume also a second order dependent on the H^+ concentration.

The rate with which the heterogeneous reaction

$$Al(OH)_4^-(aq) + H^+(aq) \rightarrow Al(OH)_3(s) + H_2O(l)$$

proceeds in the low supersaturation region may then be written

$$-\frac{dc}{dt} = k_r O(t)[H^+]^2[Al(OH)_4^-]^2 \quad [15]$$

where c refers to the concentration of the solute species (H^+ or aluminate, k_r is the rate constant, and $O(t)$ is the total surface of a constant number of growing particles per unit solution volume at time t. For the linear growth rate $\dot{R} = dR/dt$ where R is a linear dimension of the growing particle we may then write

$$\dot{R} = k'_r[H^+]^2[Al(OH)_4^-]^2. \quad [16]$$

Measurements of the linear growth rate of gibbsite seeds in supersaturated aluminate solutions by King (31) and Misra and White (32) also showed a second order dependence on aluminate concentration.

King concluded from his measurements that the order in H^+ was also two and proposed a simple mechanism which included the formation of a dimer:

$$2Al(OH)_4^- \rightleftarrows Al_2(OH)_7^- + OH^-$$

(fast; equilibrium)

$$Al_2(OH)_7^- + H^+ \rightarrow 2Al(OH)_3(s) + H_2O$$

(slow).

This mechanism predicts a second order in $[Al(OH)_4^-]$ and $[H^+]$, but if we choose the reaction $Al_2(OH)_7^- \rightarrow 2Al(OH)_3(s) + OH^-$ as the rate-determining step a first order with respect to $[H^+]$ would be found.

Equation [16] may be transcribed in the form

$$\dot{R} = k''_r \Pi^2 \quad [17]$$

where at constant pH and ionic strength, Π is proportional to the aluminate activity (concentration). The more fundamental theories of crystal growth yield expressions for the growth rate of the type $\dot{R} = f(\Pi)$. The spiral growth model of Burton *et al.* (33) applied by Bennema (34) to crystal growth from solution predicts $\dot{R} \propto (\Pi - 1)^2$ at low relative supersaturation. However, the conditions under which our experiments were performed were quite different and the two-dimensional nucleation models, including the mononuclear

(35) and the polynuclear (35–37) models, offer a better basis for comparison. Theories based on these surface nucleation models suggest the following general expression for the linear growth rate (37)

$$\dot{R} = \text{constant } (\ln \Pi)^x \exp[-B/\ln \Pi] \quad [18]$$

where x can vary over a wide range. Over a limited range of supersaturation Eq. [18] shows $\dot{R} \propto \Pi^2$ or $R \propto \Pi$ when a dimer is assumed to be the growth unit. At present we lack sufficient experimental information to attempt any serious analysis of the growth kinetics of bayerite on the basis of a surface nucleation model. Finally we note that if the more empirical approaches (38–41) to the kinetics of simple sparingly soluble salts (e.g., AgCl, $BaSO_4$) are applied, agreement with experimental observation is only obtained if we assume the growth unit to be a dimer $Al_2(OH)_n^{6-n}$.

CONCLUSIONS

(a) The acid titration experiments confirm the general view that $Al(OH)_4^-$ is the main Al(III)-bearing species in aluminate solutions.

(b) Relaxation studies at constant pH indicate that at high supersaturations (X = pH + $pAl_T \leqslant 12$) a two stage process takes place in which thermodynamically less stable (amorphous phase) pseudo-boehmite forms first and later on bayerite which nucleates heterogeneously on pseudo-boehmite surfaces. At low supersaturations ($X > 12.55$) only bayerite forms and the regularly decreasing relaxation time with increasing supersaturation is explained by the effect of supersaturation on the induction time characteristic of non-steady-state nucleation. At intermediate supersaturations the relaxation behavior is explained by a combined effect of decreased growth of pseudo-boehmite and retarded growth of bayerite by formation of pseudo-boehmite on its surface. This description also explains the position of the extrema in the relaxation time versus supersaturation curves. It is interesting to note that in entirely different systems similar retarding effects were observed. In the work of Feenstra *et al.* (48, 49) on fluorinated calcium- and strontiumhydroxyapatites a maximum in the relaxation time was observed between the formation of pure hydroxyapatites and fluorinated apatites. This retarding effect may also be explained by formation, at low fluoride concentrations, of a fluoride apatite phase on the precursor phase thereby retarding its growth. The slightly lower relaxation times at higher pAl_T and thus higher pH (constant supersaturation) might be due to lower interfacial tensions due to adsorption effects.

(c) Some simple calculations were performed to show that measurements of induction times for bayerite far from pH_{pzc} may also show extrema in the relaxation-supersaturation curves and lead to information on the absorption properties (interfacial tension) of the precipitating phase.

(d) The growth of bayerite may be described by the rate equation,

$$-\frac{dC_{Al}}{dt} = k_r O(t)[H^+]^2[Al(OH)_4^-]^2$$

where the reaction order of the H^+ ion concentration is derived from seed experiments in which the total surface remains essentially constant during growth. This rate equation was compared with the prediction of the dependence of linear growth rates on supersaturation by a number of crystal growth theories. It is in qualitative agreement with the theory based on a surface reaction controlled model. A model based on the incorporation of a dimeric Al(III)-bearing species by the growing bayerite is also consistent with the experimental results.

REFERENCES

1. Stol, R. J., van Helden, A. K., and de Bruyn, P. L., *J. Colloid Interface Sci.* **57**, 115 (1976).
2. Stol, R. J., Doctoral Thesis, Utrecht (1978).
3. Dousma, J., Doctoral Thesis, Utrecht (1979).
4. Moolenaar, R. J., Evans, J. C., and McKeever, L. D., *J. Phys. Chem.* **74**, 3629 (1970).

5. Glastonburry, J. R., *Chem. Ind.* **6,** 121 (1969).
6. Eremin, N. I., Volokhov, Yu. A., and Mironov, V. E., *Russ. Chem. Rev.* (Engl. Transl.) **43,** 92, 1974.
7. Söhnel, O., *J. Cryst. Growth* **57,** 101 (1982).
8. Rosmalen, G. M. van, Doctoral Thesis, Delft (1981).
9. Mullin, J. W., "Crystallisation," p. 207. Butterworth, London, 1972.
10. Matijević, E., *Progr. Colloid Polym. Sci.* **61,** 24 (1976).
11. Matijević, E., *J. Colloid Interface Sci.* **58,** 374 (1977).
12. Hook, A. van, "Crystallisation," p. 4. Reinhold, New York, 1961.
13. Ostwald, W., *Z. Phys. Chem.* **22,** 289 (1897).
14. Feenstra, T. P. L. M., Doctoral Thesis, Utrecht (1980).
15. Bérubé, Y. G., and de Bruyn, P. L., *J. Colloid Interface Sci.* **27,** 305 (1968).
16. Vermeulen, A. C., Geus, J. W., Stol, R. J., and de Bruyn, P. L., *J. Colloid Interface Sci.* **51,** 449 (1975).
17. Davies, C. W., *J. Chem. Soc.* 2093 (1938).
18. Brosset, C., Biedermann, G., and Sillén, L. G., *Acta Chem. Scand.* **8,** 1917 (1954).
19. Hem, J. D., and Roberson, C. E., Geological Survey Water Supply paper 1827.A (1972).
20. Brosset, C., *Acta Chem. Scand.* **6,** 910 (1952).
21. Plumb, R. C., and Swaine, J. W., Jr., *J. Phys. Chem.* **68,** 2057 (1964).
22. Stranski, I. N., and Totomanow, D., *Z. Phys. Chem. A* **163,** 399 (1933).
23. Gutzow, I., and Toschev, S., *Krist. Techn.* **3,** 485 (1968).
24. Dunning, W. J., *in* "Nucleation" (A. C. Zettlemoyer, Ed.), p. 1. Marcel Dekker, New York, 1969.
25. Toschev, S., *in* "Crystal Growth: An Introduction" (P. Hartman, Ed.), p. 1. North Holland, Amsterdam, 1973.
26. Nielsen, A. E., and Söhnel, O., *J. Cryst. Growth* **11,** 233 (1971).
27. Lippens, D. C., and Steggerda, J. J., *in* "The Physical Chemistry of Catalysts and Adsorbents" (D. G. Rinsen, Ed.), p. 184. Academic Press, New York.
28. Parks, G. A., *Chem. Rev.* **65,** 177 (1965).
29. Gindt, R., and Kern, R., *Ber. Bunsenges. Phys. Chem.* **72,** 459 (1965).
30. Stol, R. J., and de Bruyn, P. L., *J. Colloid Interface Sci.*. **75,** 185 (1980).
31. King, W. R., *Proc. Sess. Alme Ann. Meet. 102nd* **2,** 551 (1973).
32. Misra, C., and White, F. T., *Chem. Eng. Progr. Symp. Ser.* **67,** 53 (1971).
33. Burton, W. K., Cabrera, N., and Frank, F. C., *Phil. Trans. Roy. Soc.* **243,** 299 (1951).
34. Bennema, P., *J. Crystal Growth* **I,** 278 (1967), **24/25,** 76 (1974).
35. Nielsen, A. E., "Kinetics of Precipitation." Pergamon Press, New York, 1964.
36. Weeks, J. D., and Gilmer, G. H., *Adv. Chem. Phys.* **XL,** 157 (1979).
37. Garside, J., *in* "Crystal Growth and Materials" (E. Kaldis and H. J. Scheel, Eds.), p. 484. North Holland, Amsterdam, 1977.
38. Nancollas, G. H., *Adv. Colloid Interface Sci.* **10,** 215 (1979).
39. Davies, C. W., and Jones, A. L., *Trans. Faraday Soc.* **51,** 812 (1955).
40. Reich, R., and Kahlweit, M., *Der. Bunsenges. Phys. Chem.* **72,** 66 (1968).
41. Walton, A. G., *J. Phys. Chem.* **67,** 1920 (1963).
42. Deželic, N., Dikinski, N., and Wolf, R. H. H., *J. Inorg. Nucl. Chem.* **33,** 791 (1971).
43. Raupach, M., *Aust. J. Soil. Res.* **1,** 28 (1963).
44. Russell, A. S., Edwards, J. D., and Taylor, C. D., *Trans. Amer. Inst. Min. Met. Eng.* **203,** 1123 (1955).
45. Kittrich, J. A., *Soc. Sci. Soc. Amer. Proc.* **30,** 595 (1966).
46. Feitknecht, W., and Schindler, D., *Pure Appl. Chem.* **6,** 130 (1963).
47. Berecz, E., and Szite, L., ICSOBA, 1969, *Banyasz Kohasz Kohászati Lapok* **103,** 37 (1970).
48. Feenstra, T. P., van Straten, H. A., and de Bruyn, P. L., *J. Colloid Interface Sci.* **80,** 255 (1981).
49. Van den Hoek, W. G. M., Feenstra, T. P., and de Bruyn, P. L., *J. Phys. Chem.* **84,** 3312 (1980).